



## Application of flash GC e-nose and FT-NIR combined with deep learning algorithm in preventing age fraud and quality evaluation of pericarpium citri reticulatae

Yuwen Qin<sup>a,b,1,2</sup>, Qi Zhao<sup>a,b,1,2</sup>, Dan Zhou<sup>a,b,1,2</sup>, Yabo Shi<sup>c</sup>, Haiyan Shou<sup>a,b</sup>, Mingxuan Li<sup>c</sup>, Wei Zhang<sup>c,d,e,\*</sup>, Chengxi Jiang<sup>a,b,\*</sup>

<sup>a</sup> College of Pharmacy, Wenzhou Medical University, Wenzhou 325035, China

<sup>b</sup> Jiuhuashan Polygonati Rhizoma Research Institute, Chizhou 247100, China

<sup>c</sup> College of Pharmacy, Nanjing University of Chinese Medicine, Nanjing 210023, China

<sup>d</sup> College of Pharmacy, Anhui University of Chinese Medicine, Anhui 230012, China

<sup>e</sup> Anhui Province Key Laboratory of Traditional Chinese Medicine Decoction Pieces of New Manufacturing Technology, China

### ARTICLE INFO

#### Keywords:

Pericarpium citri reticulatae  
Quality evaluation  
Food fraud  
FT-NIR  
Deep learning  
CNN-LSTM

### ABSTRACT

Pericarpium citri reticulatae (PCR) is the dried mature fruit peel of *Citrus reticulata* Blanco and its cultivated varieties in the Brassicaceae family. It can be used as both food and medicine, and has the effect of relieving cough and phlegm, and promoting digestion. The smell and medicinal properties of PCR are aged over the years; only varieties with aging value can be called “Chenpi”. That is to say, the storage year of PCR has a great influence on its quality. As the color and smell of PCR of different storage years are similar, some unscrupulous merchants often use PCRs of low years to pretend to be PCRs of high years, and make huge profits. Therefore, we did this study with the aim of establishing a rapid and nondestructive method to identify the counterfeiting of PCR storage year, so as to protect the legitimate rights and interests of consumers. In this study, a classification model of PCR was established by e-eye, flash GC e-nose, and Fourier transform near-infrared (FT-NIR) combined with machine learning algorithms, which can quickly and accurately distinguish PCRs of different storage years. DFA and PLS-DA models were established by flash GC e-nose to distinguish PCRs of different ages, and 8 odor components were identified, among which (+)-limonene and  $\gamma$ -terpinene were the key components to distinguish PCRs of different ages. In addition, the classification and calibration model of PCRs were established by the combination of FT-NIR and machine learning algorithms. The classification models included SVM, KNN, LSTM, and CNN-LSTM, while the calibration models included PLSR, LSTM, and CNN-LSTM. Among them, the CNN-LSTM model built by internal capsule had significantly better classification and calibration performance than the other models. The accuracy of the classification model was 98.21 %. The  $R^2$  of age, (+)-limonene and  $\gamma$ -terpinene was 0.9912, 0.9875 and 0.9891, respectively. These results showed that the combination of flash GC e-nose and FT-NIR combined with deep learning algorithm could quickly and accurately distinguish PCRs of different ages. It also provided an effective and reliable method to monitor the quality of PCR in the market.

**Abbreviations:** PCR, pericarpium citri reticulatae; DFA, discriminant factor analysis; PLS-DA, partial least squares discriminant analysis; CNN-LSTM, convolutional neural network- long short-term memory; FT-NIR, Fourier transform near-infrared; MSC, multiplicative scatter correction; SNV, standard normal transformation; SG, Savitzky-Golay; 1d, first derivative; 2d, second derivative; SVM, support vector machine; KNN, k-nearest neighbor.

\* Corresponding authors at: College of Pharmacy, Nanjing University of Chinese Medicine, Nanjing 210023, China (W. Zhang). College of Pharmacy, Wenzhou Medical University, Wenzhou 325035, China (C. Jiang).

E-mail addresses: [114380@wmu.edu.com](mailto:114380@wmu.edu.com) (Y. Qin), [1297909219@qq.com](mailto:1297909219@qq.com) (Q. Zhao), [zd15029576186@126.com](mailto:zd15029576186@126.com) (D. Zhou), [897129498@qq.com](mailto:897129498@qq.com) (Y. Shi), [1072731376@qq.com](mailto:1072731376@qq.com) (H. Shou), [jstzlmx@163.com](mailto:jstzlmx@163.com) (M. Li), [zhangwei@ahtcm.edu.cn](mailto:zhangwei@ahtcm.edu.cn) (W. Zhang), [jiangchengxi@126.com](mailto:jiangchengxi@126.com) (C. Jiang).

<sup>1</sup> Co-first authors: Yuwen Qin, Qi Zhao, and Dan Zhou.

<sup>2</sup> These authors contributed equally to this work.

<https://doi.org/10.1016/j.fochx.2024.101220>

Received 1 November 2023; Received in revised form 4 February 2024; Accepted 8 February 2024

Available online 12 February 2024

2590-1575/© 2024 Published by Elsevier Ltd. This is an open access article under the CC BY-NC-ND license (<http://creativecommons.org/licenses/by-nc-nd/4.0/>).

## 1. Introduction

Pericarpium citri reticulatae (PCR) is the dried mature peel and its cultivated varieties of *Citrus reticulata* Blanco. PCR has been used as medicine and food for more than 2000 years (Pan, Zhang, Xu, Yin, Gu, & Yu, 2022). PCR mainly contains volatile oil, flavonoids, phenolic acids and alkaloids, which has good antiasthmatic, anti-inflammatory and antioxidant activities (Bian et al., 2022; Zhang et al., 2020). It is used to promote digestion, expectorate and relieve coughs. It is widely used in food, beverage, seasoning processing and fruit tea, fruit wine production process (Yi, Dong, Liu, Yi, & Zhang, 2015). In the process of using PCR, people also summed up the empirical law of “the longer the aging time, the better the quality”. It is considered that the medicinal and edible efficacy of PCR is better after aging. Modern studies show that the volatile components in the low boiling range of PCR are lost during aging, and the contents of total flavonoids and hesperidin increase with aging time, which not only reduces its irritation, but also makes its flavor more mellow. Therefore, there is the saying that “50 g PCR is equal to the value of 50 g gold, and one hundred years PCR is worth more than gold”. In short, aging year is one of the most important criteria to measure the quality of PCR.

At present, the annual processing volume of PCR has exceeded 1000 tons, and the annual export volume has reached more than 400 tons. The prices of PCR vary greatly in different years, huge profits and low counterfeiting costs make the market full of inferior phenomena such as dyeing and adulteration, such as the use of PCR with low storage vintages to pass off as PCR with high storage vintages, which not only seriously infringes upon the interests of consumers, but also has a bad impact on food safety and quality control. However, the conventional analysis methods such as LC-MS and GC-MS are complex and cannot realize real-time high-throughput non-destructive testing and fast discrimination (Luo et al., 2019). The analysis model based on chromatography discrimination is no longer applicable due to the improvement of dyeing technology. Therefore, there is an urgent need to develop rapid and accurate discrimination techniques and analysis methods to adapt to the current large circulation mode to quickly distinguish the year and quality of PCR.

In recent years, electronic nose (e-nose) and near infrared (NIR) spectroscopy techniques have also become popular in food quality evaluation. They are high-speed, convenient, stability, low-cost, and do not require any sample pretreatment (Bai, Fang, Zhang, & Fan, 2022; Guo et al., 2023). This provides a new quality identification technique for functional foods with special flavors such as PCR. E-nose can reflect the flavor characteristics and main flavor components of the sample as a whole, and form a characteristic “odor fingerprint” to characterize the quality and flavor changes of PCR during aging (Li et al., 2022; Liu, Xiao, Zhang, & Sun, 2023). NIR spectroscopy can provide a large number of spectral features, so it is often combined with machine learning algorithms in order to be better applied (Azadnia, Rajabipour, Jamshidi, & Omid, 2023; Rong, Wang, Ying, Zhang, & Zhang, 2020). Compared to traditional machine learning algorithms, deep learning methods can handle large and complex data, adapt to a wide variety of data, automate feature extraction, and can improve their performance and accuracy by continuously learning new data. For example, because of its unique hidden layer structure, convolution neural network (CNN) can extract features automatically, so it has been successfully applied to the geographical source identification of food (Cruz Ulloa, Krus, Barrientos, Cerro, & Valero, 2022; Nasiri, Yoder, Zhao, Hawkins, Prado, & Gan, 2022).

For the purpose of achieving rapid and accurate identification of storage year falsification in PCR, flash GC e-nose and FT-NIR techniques were used to characterize the dynamic changes of flavor fingerprint and spectral characteristics during the aging process of PCR, and the main flavor components were identified. Based on the deep learning model, the age discrimination model and the prediction model of characteristic component content were established, which can be applied to the

evaluation of the authenticity and superiority of PCR in the market. It also provides technical and method support for rapid non-destructive testing and adulteration identification of PCR and other functional foods with special flavor.

## 2. Materials and methods

### 2.1. Samples and reagents

We collected PCRs of different ages from medicinal materials market. Among them, there were 25 samples aged 0-year-old, 30 samples aged 5, 10, 15, 20, 25 years old, respectively, and 29 samples aged 30 years old. All the collected samples were identified by Prof. Chengxi Jiang of Wenzhou Medical University as the dried mature pericarp of *Citrus reticulata* Blanco of Rutaceae plant and its cultivated varieties.

The *n*-alkane mixture (C<sub>6</sub>~C<sub>16</sub>) was purchased from RESTEK Co. Ltd., (USA, Lot: A0142930); (+)-limonene was purchased from Shanghai Macklin Biochemical Technology Co., Ltd. (Shanghai, China, Lot: C15084208) and  $\alpha$ -pinene (Lot: PCS-22121) were purchased from Chengdu Zhibiao Pure Biotechnology Co., Ltd. (Si chuan, China).

### 2.2. Analysis of volatile components of PCRs by flash GC e-nose

Firstly, we crushed all the PCRs, sifted the powder through 50 mesh, and stored them in a dry and dark environment for experimental use. Then the collection conditions were optimized, including sample weighing, hatching time, hatching temperature and injection volume. The final conditions are as follows: first, pour 0.5 g powder of PCRs into the 20 ml headspace bottle, then incubate 20 min at 55 °C and inhale 250  $\mu$ l of gas for analysis.

### 2.3. FT-NIR determination of PCRs

In this step, we collected the NIR spectra of the external skin and internal capsule of PCRs respectively. Using Antaris II FT-NIR spectrometer (Seamer Fisher Technology, USA) to collect spectral information of samples in diffuse reflection mode (Li et al., 2021). Three points were randomly selected from the external skin and internal capsule of each sample, and the average value of three measurements was taken as the original spectrum. The spectrum acquisition range was 10,000 ~ 4000  $\text{cm}^{-1}$ , the resolution was set to 16  $\text{cm}^{-1}$ , and each spectrum was scanned 32 times.

### 2.4. Spectral preprocessing and data set partition

There are many problems in the original NIR spectrum data, such as noise, baseline drift, spectral overlap and so on, so we use preprocessing method to improve the accuracy and reliability of the model. The preprocessing methods include multiplicative scatter correction (MSC), standard normal transformation (SNV), Savitzky-Golay (SG), first derivative (1d) and second derivative (2d) (Barra, Briak, & Kebede, 2022). MSC is mainly used to eliminate the absorption and oblique shift caused by light scattering (Jiao, Li, Chen, & Fei, 2020), SNV is used to eliminate the multiplicative interference of scattering and particle size, and 1d and 2d are usually used to eliminate vertical offset and linear tilted baseline (Zhang, Sun, Li, Zeng, & Wang, 2021).

Generally, reasonable sample set partition can effectively improve the prediction accuracy of the model. Based on Kennard-Stone algorithm (Morais, Santos, Lima, & Martin, 2019), 204 samples of PCRs were divided into 150 calibration sets and 54 validation sets.

### 2.5. Chemometrics analysis

#### 2.5.1. Multivariate statistical analysis

The principal component analysis (PCA) and discriminant factor analysis (DFA) models are based on the multivariate statistical analysis

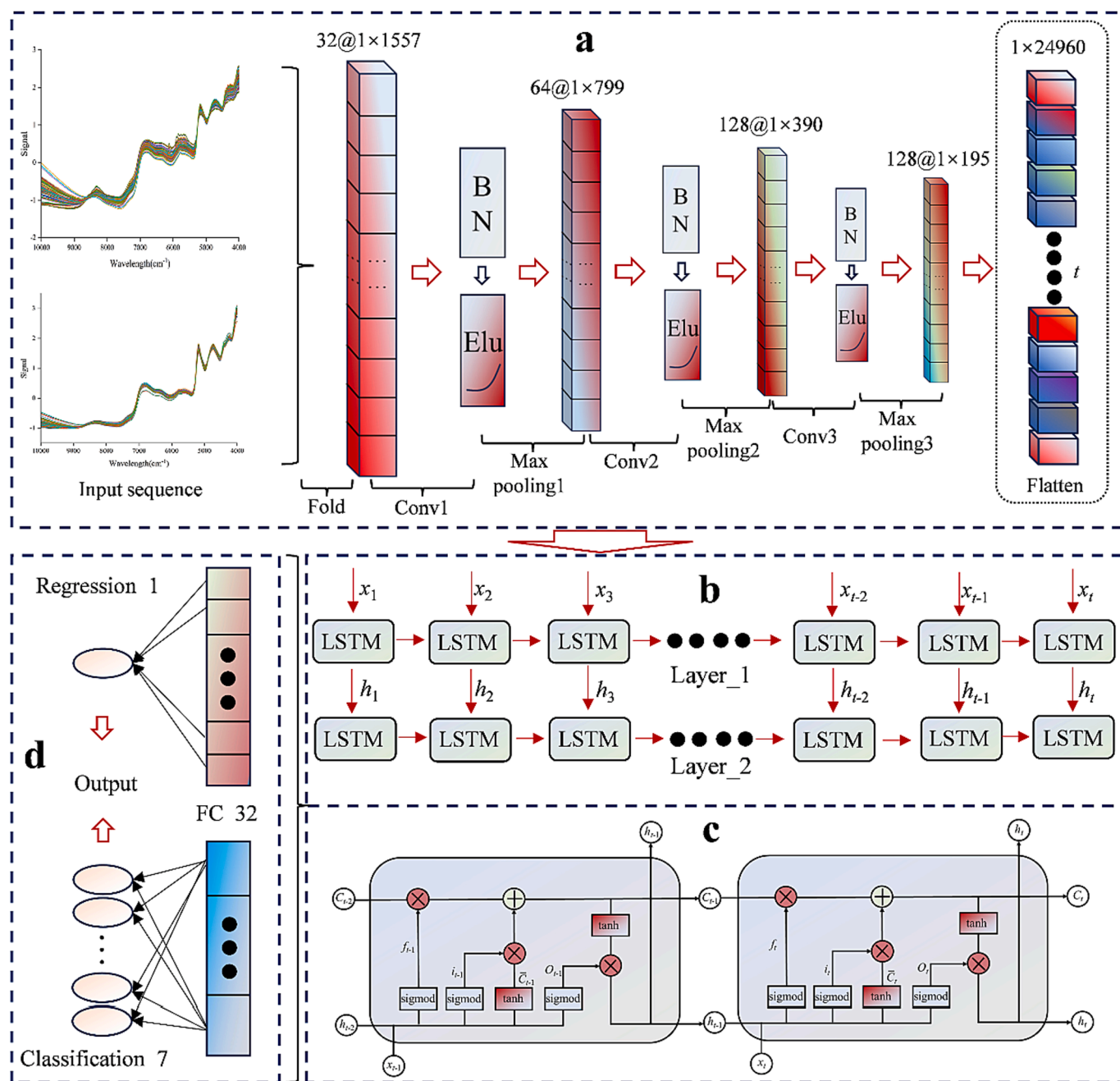


Fig. 1. Structural schematic diagram of CNN-LSTM model: (a) the structure of CNN, the name of each layer at the bottom, the size of the output data, and the size of the convolution kernel at the top; (b) the operation mode of LSTM; (c) the structure of LSTM; (d) full connection layer and output layer.

module built into the e-nose software, and the partial least squares discriminant analysis (PLS-DA) model is carried out by the SIMCA-P 14.1 software.

Among them, PCA is a commonly used unsupervised classification and statistical method, which can reduce dimensionality and extract features from high-dimensional data (Fuentes et al., 2023). DFA is a supervised classification method, which is mainly used to find the linear combination that can classify the observed objects most effectively (Zhang et al., 2023). PLS-DA is mainly used to deal with multivariable data with classification tags. It uses PLS method to establish a prediction model (Zeng et al., 2021), projects the input data into a low-dimensional space, and then uses classification label information to find the best discriminant surface. The multivariate statistical analysis method mainly classifies and predicts the data obtained from the e-nose.

### 2.5.2. Machine learning algorithm

The support vector machine (SVM) and k-nearest neighbor classification (KNN) models are constructed by Matlab R2021a software, which mainly classify and predict the NIR spectrum data.

SVM is a supervised learning algorithm, which maps data to high-dimensional feature space and finds out the hyperplanes that can best divide different categories of data (Wang, Jiang, Mo, Tang, & Lv, 2020; Yuan et al., 2020). The technology based on kernel function can solve nonlinear problems. KNN is a simple and effective machine learning algorithm for classification and regression (Dong, Wang, Weng, Yuan, & Yang, 2021). Based on the distance measure between samples, it predicts by finding the K neighbors closest to the data to be tested (Balabin & Safieva, 2011).

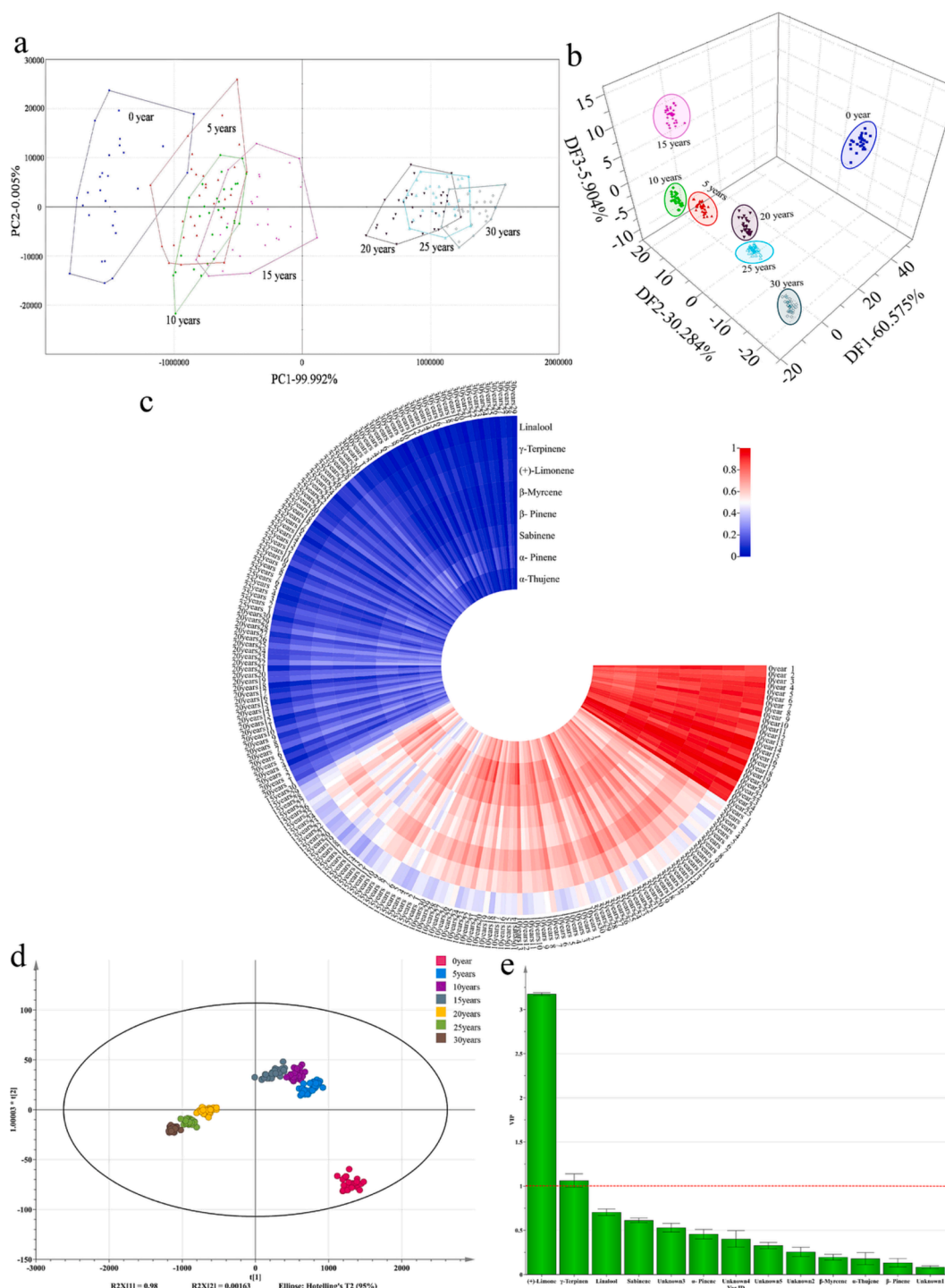


Fig. 2. E-nose analysis of PCRs: PCA model (a), DFA model (b), flavor heat map (c), PLS-DA model (d), VIP score (e).

### 2.5.3. Deep learning algorithm—CNN-LSTM

CNN-LSTM is a new network structure which combines convolution neural network (CNN) with long short-term memory (LSTM). CNN can extract effective features from data, while LSTM is a variant of cyclic neural network (RNN). It can not only find the interdependence of data in time series data, but also automatically detect the best pattern suitable for related data. The combination of the two can improve the accuracy and stability of the model, and can classify and regression predict the near infrared spectrum at the same time. The model is constructed by Matlab R2021a software.

Fig. 1 shows the structure of the CNN-LSTM model. Fig. 1(a) is the

structure of CNN, which mainly includes data input, convolution layer, batch normalization layer, eLU activation function, maximum pool layer and flat layer. Convolution layer is the core of CNN and has good feature extraction ability for data with local features. Batch normalization (BN) method is added to each convolution, which can normalize the output of each convolution to stabilize the learning process. The activation function of the convolution layer uses the Elu function, which is an improved ReLU function. When the input is negative, the output value has a certain anti-interference ability, which can eliminate the problem of ReLU death (Yu, Ma, Chen, Li, & Li, 2020). Its mathematical expression can be found in formula (1):

$$Elu(x) = \begin{cases} x, & x > 0 \\ a(e^x - 1), & x \leq 0 \end{cases} \quad (1)$$

Where  $x$  is the input value and  $a$  is the weighting coefficient. After each convolutional layer, select the maximum pooling area through the maximum pooling layer to reduce the number of parameters, reduce computational costs, and prevent overfitting. Finally, the output of the pooling layer is converted into one-dimensional vectors through the flat layer and transmitted to the LSTM unit structure.

Compared to traditional RNNs, which are prone to gradient vanishing and exploding, LSTM has added a cell state on top of it to preserve long-term states. The cell state is controlled by important “gate” structures, namely forgetting gate, input gate, and output gate. Fig. 1(b) shows the operation mode of LSTM, and Fig. 1(c) shows the internal structure of LSTM. The input gate is used to update the information of the cell state, as calculated in formula (2) and (3):

$$i_t = \sigma(W_i[h_{t-1}, x_t] + b_i) \quad (2)$$

$$\tilde{C}_t = \tanh(W_c[h_{t-1}, x_t] + b_c) \quad (3)$$

The forgetting gate is mainly used to control the retention of information in the cell state, which is calculated as shown in formula (4):

$$f_t = \sigma(W_f[h_{t-1}, x_t] + b_f) \quad (4)$$

The output gate is mainly used to control the output information, and their calculation method is such as formula (5) ~ (7):

$$O_t = \sigma(W_o[h_{t-1}, x_t] + b_o) \quad (5)$$

$$h_t = O_t \cdot \tanh(C_t) \quad (6)$$

$$\tilde{C}_t = f_t \cdot C_{t-1} + i_t \cdot \tilde{C}_t \quad (7)$$

Among them,  $W_i$ ,  $W_f$ ,  $W_o$ ,  $W_c$  are the weight,  $b_i$ ,  $b_f$ ,  $b_o$ ,  $b_c$  are the bias,  $f_t$  is the input of the forgetting gate,  $h_{t-1}$  is the output of the basic cell of the  $t-1$  moment,  $x_t$  is the input of the current moment,  $C_t$  is the updated output of the cell state, the product of  $i_t$  and  $\tilde{C}_t$  is the output of the input gate, and  $h_t$  is the output of the hidden state.  $\sigma$  is a sigmoid function and  $\tanh$  is a hyperbolic tangent function. Their mathematical expressions are shown in formula (8) and (9):

$$\sigma(x) = 1/(1 + e^{-x}) \quad (8)$$

$$\tanh(x) = (e^x - e^{-x})/(e^x + e^{-x}) \quad (9)$$

Fig. 1(d) is the output layer of the CNN-LSTM, including the full connection (FC) layer and the output layer, which is output by the classification layer when the classification task is performed and by the regression layer when the regression task is performed. All the model parameters can be obtained from Table S1.

## 2.6. Model evaluation

The classification model of this paper is mainly evaluated by accuracy (Acc), precision (Pr), recall rate (Re) and F1 score (F1). Acc refers to the proportion of the total number of predicted correct results, Pr examines whether the identified positive samples are reliable, Re examines whether they are sensitive to positive samples, and F1 is an index that takes into account Pr and Re. The specific calculation method is shown in the formula (10) ~ (13):

$$Acc = \frac{TP + TN}{TP + TN + FP + FN} \times 100\% \quad (10)$$

$$Pr = \frac{TP}{TP + FP} \times 100\% \quad (11)$$

$$Re = \frac{TP}{TP + FN} \times 100\% \quad (12)$$

$$F1 = \frac{2 * (Pr * Re)}{Pr + Re} \times 100\% \quad (13)$$

Where TP represents the number of positive samples correctly classified; TN represents the number of negative samples that are correctly classified; FP represents the number of negative samples misclassified as positive samples; FN represents the number of positive samples misclassified as negative samples.

The regression model mainly takes correlation coefficient ( $R^2$ ), root mean square error (RMSE) and relative prediction error (RPD) as evaluation indexes. The closer to 1  $R^2$  is, the smaller the RMSE is, which indicates that the accuracy of the model is higher. Generally,  $RPD > 3$  indicates that the model has excellent prediction ability.

## 3. Results and discussion

### 3.1. E-nose analysis of PCRs

#### 3.1.1. Analysis of odor characteristics of PCRs of different ages by flash GC e-nose

The standard solution of  $n$ -alkanes was used to calibrate the chromatographic peak retention time ( $t_R$ ) of each sample into Kovats retention index (RI). A total of 13 odor components were identified. 8 flavor compounds were identified by AroChemBaseNist standard database and comparison of reference materials (Table S2), including  $\alpha$ -thujene,  $\alpha$ -pinene, sabinene,  $\beta$ -pinene,  $\beta$ -myrcene, (+)-limonene,  $\gamma$ -terpinene, and linalool. The concentration of the identified compound is expressed in mg/g (Table S3), which is calculated based on the equivalent of (+)-limonene. It can be seen from Table S2 that (+)-limonene has a special orange flavor, and its content is the highest in PCRs of different ages, all above 80 %, indicating that the aroma of PCRs is mainly contributed by (+)-limonene. In addition, PCRs is also spicy and herbal.

Fig. S1 shows the odor chromatogram of PCRs of different ages. It can be seen that with the increase of age, the intensity of odor chromatographic peak of PCRs decreases gradually. Fig. 2(c) is a flavor heat map based on the concentrations of 8 identified compounds. It can be seen that the content of all components is the highest in 0-year-old samples, and then decreases gradually. However, the contents of 5–15 years old samples were similar, and 20–30 years old samples, indicating that the smell of PCRs was similar in some storage stages.

#### 3.1.2. Distinguish PCRs of different ages based on flash GC e-nose

Based on the results of electronic nose, we established a PCA (Fig. 2a) model to distinguish and identify PCRs of different ages. It can be seen that there is a certain degree of intersection between the 0 ~ 15 years samples and between the 20 ~ 30 years samples, indicating that they have some similarity in odor. The 0 ~ 15 years samples and 20 ~ 30 years samples can be completely separated, implying that 15–20 years is an important inflection point of PCR odor composition (Fig. 2a). In the DFA diagram, all samples can be completely distinguished, the contribution rate of the first three discriminant factors reached 96.763 %, and the 0-year-old samples are the farthest from other samples, indicating that DFA can be used to distinguish PCRs of different ages (Fig. 2b).

It can be seen from Fig. 2(d) that PCRs of different ages can be well distinguished by PLS-DA. Fig. S2 is a PLS-DA model fitting diagram, in which the interpretation rate parameter  $R^2Y$  is 0.752 and the prediction ability parameter  $Q^2$  is 0.741, indicating that the PLS-DA model has reliable performance (Du et al., 2021). The PLS-DA model was randomly arranged 200 times for permutation test, and the intercept of the fitting line of  $R^2$  and  $Q^2$  was less than 0.05, which indicated that the PLS-DA model was not over-fitted (Becerra-Martínez et al., 2017).

Variable importance (VIP) was further used to identify the main odor

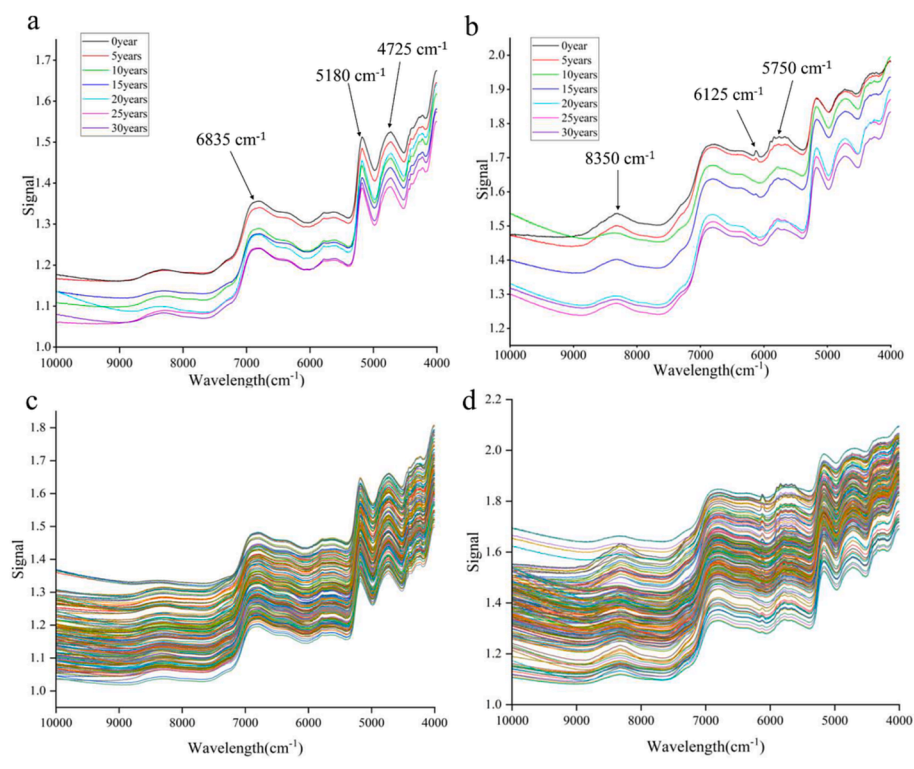


**Fig. 3.** NIR spectra of external skin(a) and internal capsule(b) of PCRs of different ages; superposition spectra of external skin(c) and internal capsule(d) of all samples.

difference components among PCRs of different ages. The predictive value of VIP can directly reflect the contribution of each variable to model classification. The larger the VIP, the greater the contribution of variables to the differentiation of different groups of samples. In general, a VIP value greater than 1 can be considered a key variable between different groups. It can be seen from Fig. 2(e) that the VIP of (+)-limonene and  $\gamma$ -terpinene are greater than 1, which may be the odor difference markers to distinguish PCRs of different ages.

(+)-Limonene is the largest odor component in PCRs. It is a natural functional monoterpene with antioxidant, anti-inflammatory, and gastroprotective effects (Anandakumar et al., 2020). At the same time, because of its pleasant orange aroma, (+)-limonene is often used as an additive in the food industry. In recent years, it has been found that (+)-limonene has good tumor prevention and inhibitory activity, and has achieved good results in the prevention and treatment of various types of cancer (Araújo-Filho et al., 2021).  $\gamma$ -Terpinene has a variety of activities such as bacteriostasis, anti-tumor and regulation of gastrointestinal tract, and it can also protect the activity of antioxidant enzymes, so as to restore cell damage to a certain extent and play an antioxidant role. In summary, the pharmacological effects of odor differential markers such as (+)-limonene and  $\gamma$ -terpinene are consistent with the clinical use of PCR for the treatment of spleen and stomach disorders.

### 3.2. FT-NIR analysis of PCRs

#### 3.2.1. Original NIR characteristics of PCRs of different ages

Fig. 3 (a) and (b) are the superposition images of the external skin and internal capsule of the PCRs of different ages, respectively. We can see that there is an obvious difference between them. There are mainly three absorption peaks in the external skin spectrum, among which the absorption peak close to  $4725\text{ cm}^{-1}$  is caused by tensile vibration of C—C and C=C (Zhang et al., 2023). The absorption peak close to  $5180\text{ cm}^{-1}$  may be caused by the second overtone absorption of tensile vibration of C=O or stretching and deformation vibration of O—H (Liu

et al., 2019). The absorption peak at  $6835\text{ cm}^{-1}$  is caused by the first overtone absorption of tensile vibration of O—H (Ma et al., 2020). The production of these absorption peaks may be caused by flavonoids. In addition, there are three other absorption peaks in the spectrum of the internal capsule which are different from those of the external skin. Near  $5750\text{ cm}^{-1}$ ,  $6125\text{ cm}^{-1}$  and  $8350\text{ cm}^{-1}$ , respectively. According to the knowledge of spectral analysis, these may be caused by the tensile vibration of C—H in some aromatic compounds or the overtones produced by them (Barra et al., 2022; Zhan et al., 2017). This is because the aromatic compounds of PCRs are mostly stored in the oil chamber of the internal capsule, while these substances are rarely found in the external skin. No matter the external skin or the internal capsule, the intensity of each absorption peak basically decreases with the increase of age, which is consistent with the change law of the components detected by the e-nose, indicating that the intensity of the absorption peak is closely related to the concentration of odor components. Fig. 3(c) and (d) are the spectral superposition maps of the external skin and internal capsule of all samples, respectively. It can be seen that the spectral curves of PCRs of different ages overlap obviously and have high similarity, so we need to preprocess them to eliminate interference.

#### 3.2.2. Classification analysis based on FT-NIR

In this part, the original data of NIR spectrum are used as the input of different classification models to distinguish the PCRs of different ages. The model classification confusion matrix is shown in Fig. S3. It can be seen that no matter using external skin data as input or internal capsule data as input, CNN-LSTM model only misclassifies a small number of samples, and the classification result is obviously better than that of other models. Therefore, PCRs of different ages can be distinguished according to the results of data set distribution in CNN-LSTM model.

Fig. S4 shows the loss function curve (red) and accuracy curve (green) of LSTM and CNN-LSTM respectively. The abscissa represents the number of iterations of the training. The longitudinal coordinates of the left axis and the right axis are the loss function and the accuracy

**Table 1**  
Performance evaluation of different classification models.

Sample	Model	Data set	Acc/%	Pr/%	Re/%	F1/%
External skin	SVM	Calibration	83.81	83.57	83.98	83.77
		Validation	79.86	79.80	79.89	79.85
	KNN	Calibration	83.48	82.20	84.79	83.47
		Validation	78.16	76.70	79.00	77.83
	LSTM	Calibration	87.89	87.63	88.09	87.86
		Validation	87.11	87.79	86.61	87.19
CNN-LSTM	Calibration	100.00	100.00	100.00	100.00	
	Validation	93.77	94.23	93.37	93.80	
Internal capsule	SVM	Calibration	88.90	87.93	89.67	88.79
		Validation	88.41	88.21	88.56	88.38
	KNN	Calibration	87.54	87.24	87.77	87.51
		Validation	79.43	78.91	79.73	79.32
	LSTM	Calibration	94.30	93.87	94.68	94.28
		Validation	84.94	82.57	86.67	84.57
CNN-LSTM	Calibration	100.00	100.00	100.00	100.00	
	Validation	98.21	97.61	98.80	98.20	

respectively. It can be seen that the accuracy and loss value of LSTM model fluctuate seriously during the training process. In contrast, the loss function of CNN-LSTM model is lower, the classification accuracy is higher, and it can reach a stable state through less iterations. Then we observe the training process of the external skin and internal capsule data of the two models respectively, and find that no matter which model is selected, when using the internal capsule data for classification learning, the training curve is smoother than the outer skin, and can reach the stable state faster, and the loss function is low, and the accuracy is high. The results show that compared with the external skin, the internal capsule data is more effective in classifying PCRs of different ages, and the CNN-LSTM model has good stability and efficiency for classification.

In order to evaluate the accuracy and stability of each model more accurately, we recorded the Acc, Pr, Re and F1 of the calibration and validation sets for each model in Table 1. When classifying with external skin data, the values of Acc, Pr, Re and F1 of the validation set of CNN-LSTM model are 93.77 %, 94.23 %, 93.37 % and 93.80 % respectively, which are higher than those of the other three models and have better classification efficiency. Among them, Pr is 94.23 %, which is higher than Re, indicating that the classification result of the model for true positive is better than that of true negative. When using internal capsule

**Table 2**  
Using different calibration models to predict the age and main volatile components of PCRs.

Sample	Index	Model	Calibration			Validation		
			$R_c^2$	RMSE <sub>c</sub>	RPD <sub>c</sub>	$R_p^2$	RMSE <sub>p</sub>	RPD <sub>p</sub>
External skin	Age	PLS	0.9556	1.99	4.85	0.9566	2.07	5.09
		LSTM	0.9877	1.11	9.01	0.9819	1.26	7.53
		CNN-LSTM	0.9886	1.05	10.01	0.9862	1.15	9.09
	(+)-Limonene	PLS	0.8973	0.59	3.28	0.8667	0.65	3.14
		LSTM	0.9129	0.56	3.40	0.9063	0.63	3.27
		CNN-LSTM	0.9749	0.30	6.31	0.9728	0.34	6.16
	$\gamma$ -Terpinene	PLS	0.8891	0.03	3.17	0.8814	0.03	3.20
		LSTM	0.9367	0.03	4.35	0.9217	0.03	3.74
		CNN-LSTM	0.9798	0.02	7.13	0.9768	0.02	6.59
Internal capsule	Age	PLS	0.9647	1.85	5.42	0.9559	1.92	4.79
		LSTM	0.9782	1.47	7.77	0.9685	1.65	6.22
		CNN-LSTM	0.9914	0.89	10.99	0.9912	0.97	10.64
	(+)-Limonene	PLS	0.8874	0.62	3.14	0.8668	0.66	3.06
		LSTM	0.9168	0.55	3.47	0.9138	0.60	3.45
		CNN-LSTM	0.9887	0.21	9.48	0.9875	0.21	9.05
	$\gamma$ -Terpinene	PLS	0.9389	0.03	4.17	0.8978	0.03	3.38
		LSTM	0.9487	0.02	4.42	0.9496	0.03	4.51
		CNN-LSTM	0.9902	0.01	10.12	0.9891	0.01	9.58

data for classification, the Acc, Pr, Re, and F1 of the CNN-LSTM model reached 98.21 %, 97.61 %, 98.80 %, and 98.20 %, respectively. Among them, Pr is 97.61 %, which is lower than Re, indicating that the classification results of the model for true negative are better than true positive. By comparing the classification models of external skin and internal capsule, it is found that the CNN-LSTM classification model based on internal capsule data can identify PCRs of different ages more accurately.

### 3.2.3. Spectral preprocessing and data set partitioning

The original spectra were pretreated with MSC, SNV, SG, 1d and 2d, respectively, and the pretreatment spectra of external skin and internal capsule were shown in Figs. S5 and S6, respectively. It can be seen that different methods have different advantages in improving spectral characteristics and correcting scattered light.

Table S4 statistics the age, (+)-limonene and  $\gamma$ -terpinene data of the calibration set and the validation set, and it can be seen that the variation range of all the data of the calibration set completely covers the range of the verification set. The average value and standard deviation of test set and verification set are basically similar. These data show that the result of sample set division is reasonable and the samples selected for modeling are highly representative.

We used the PLS model to establish the calibration models of the age and two key odor components ((+)-limonene and  $\gamma$ -terpinene) of PCRs based on the pretreated data of external skin and internal capsule, respectively. The results are shown in Table S5 and S6, respectively. It can be seen that, compared with other preprocessing methods, SNV has the best calibration results for age, (+)-limonene and  $\gamma$ -terpinene, regardless of whether the external skin data or internal capsule data are used as input, which is consistent with previous studies.

### 3.2.4. Rapid prediction of age and content of key odor components in PCRs by CNN-LSTM

We determine the best pretreatment method through spectral preprocessing. In order to make the prediction model more accurate, we develop a quantitative model of CNN-LSTM, which can directly input the features extracted by CNN into LSTM for processing. This method saves the step of extracting feature wavelength and reduces the error of calibration results.

Table 2 records the comparative effects of PLSR, LSTM, and CNN-LSTM models. The results (taking the external skin as an example) show that in the age calibration model established by CNN-LSTM,  $R^2$

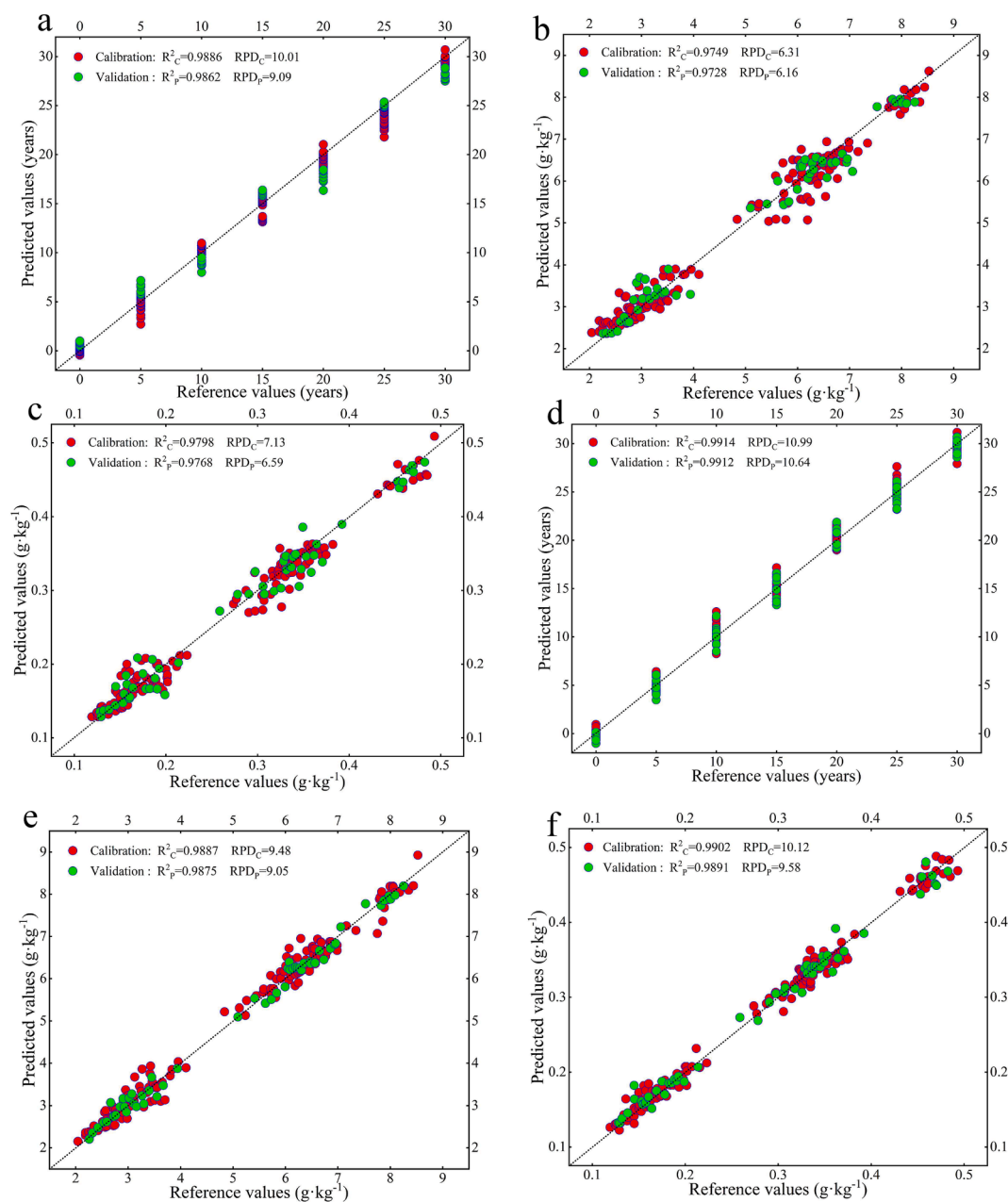


**Fig. 4.** Comparison of reference value and predicted value: (a) (b) (c) are the calibration models of age, (+)-limonene and  $\gamma$ -terpinene based on external skin; (d) (e) (f) are the calibration models of age, (+)-limonene and  $\gamma$ -terpinene based on internal capsule.

(0.9862) and RPD (9.09) are larger than PLSR and LSTM models, indicating that the accuracy of the model is higher, while RMSE (1.15) is relatively small, indicating that the error of the model is small. By observing the quantitative models of (+)-limonene and  $\gamma$ -terpinene, it is found that this rule also appears, indicating that CNN-LSTM is more accurate in predicting the age and odor components of PCRs. Then we observed the calibration model based on the data of external skin and internal capsule (taking (+)-limonene as an example). The validation set of model established by internal capsule had higher  $R^2$  (0.9875) and RPD (9.05) than that of external skin, and RMSE (0.34) was smaller, and this situation occurred in the three models at the same time. We visualize the prediction results of the age and odor composition of PCRs through CNN-LSTM (Fig. 4). We can see that in the model established through the external skin, although all the points are on the diagonal, they are slightly discrete, while in the model established through the internal capsule, all the points are closely close to the diagonal and the

degree of dispersion is low. It shows that the prediction model of age and odor components through the internal capsule is more accurate. This may be because with the increase of age, the change of the internal capsule of PCRs is more obvious than that of the external skin, and the oil chamber of PCRs is mostly in the internal capsule, and the oil chamber is the place to store aroma, so it will be more accurate to reflect the odor components through the internal capsule.

#### 4. Conclusion

In this study, the aroma changes of PCRs during storage were clarified by flash GC e-nose. The established DFA and PLS-DA models can accurately distinguish PCRs of different ages by odor components, of which two odor components ((+)-limonene and  $\gamma$ -terpinene) are considered to be the key components to distinguish PCRs of different ages. The NIR spectrum data of external skin and internal capsule of

PCRs of different ages were collected, and the classification model which could distinguish PCRs of different ages was established by using CNN-LSTM. In order to accurately evaluate the quality of PCRs of different ages, we used NIR spectrum to predict the age of PCRs, and combined the key odor components obtained by e-nose with NIR spectrum to establish a CNN-LSTM quantitative prediction model for evaluation. The results show that compared with the external skin, the model established by internal capsule data is more reliable, and compared with PLSR and LSTM, the prediction model established by CNN-LSTM has higher accuracy and robustness.

The method established in this study realized the precise distinction and quality evaluation of PCRs of different ages, which can quickly and effectively prevent the counterfeiting of PCRs in the market. Compared with traditional detection methods, flash GC e-nose and FT-NIR technology have great potential in identifying food fraud. By combining with deep learning algorithm, food can be evaluated more quickly and accurately. The method established in this study is suitable for quickly tracking adulteration in food to ensure the authenticity of the product. It provides a useful technical way to maintain the stability of the food consumption market and protect the interests and health of consumers. A quantitative validation study of the most critical volatile components ((+)-limonene and  $\gamma$ -terpinene) for distinguishing PCR with different storage times will be carried out at a later stage of the program. The relevant odor markers of PCR will be further identified with a view to achieving rapid identification and quality control of PCR with different storage times.

## Funding

This research study was funded by the 2023 Special Funding for Discipline Building - Pharmacy (No. 437602303), Research on Quality Control and Enhancement of Traditional Chinese Medicines such as *Curcumae Rhizoma* Formulated granules (No. KJHX2009).

## CRedit authorship contribution statement

**Yuwen Qin:** Writing – original draft, Writing – review & editing. **Qi Zhao:** Writing – original draft. **Dan Zhou:** Data curation, Methodology. **Yabo Shi:** Writing – original draft, Writing – review & editing. **Haiyan Shou:** Data curation, Methodology. **Mingxuan Li:** Methodology. **Wei Zhang:** Conceptualization. **Chengxi Jiang:** Funding acquisition.

## Declaration of competing interest

The authors declare that they have no known competing financial interests or personal relationships that could have appeared to influence the work reported in this paper.

## Data availability

Data will be made available on request.

## Appendix A. Supplementary data

Supplementary data to this article can be found online at <https://doi.org/10.1016/j.fochx.2024.101220>.

## References

- Anandakumar, P., Kamaraj, S., & Vanitha, M. K. (2020). D-limonene: A multifunctional compound with potent therapeutic effects. *Journal of Food Biochemistry*, 45(1): e13566. doi: 10.1111/jfbc.13566. Epub 2020 Dec 1. PMID: 33289132.
- Araújo-Filho, H. G., Dos Santos, J. F., Carvalho, M. T. B., Picot, L., Fruitier-Arnaudin, I., Grout, H., Quintans-Júnior, L. J., & Quintans, J. S. S. (2021). Anticancer activity of limonene: A systematic review of target signaling pathways. *Phytotherapy Research*, 35(9):4957-4970.
- Azadnia, R., Rajabipour, A., Jamshidi, B., & Omid, M. (2023). New approach for rapid estimation of leaf nitrogen, phosphorus, and potassium contents in apple-trees using Vis/NIR spectroscopy based on wavelength selection coupled with machine learning. *Computers and Electronics in Agriculture*, 207, Article 107746. <https://doi.org/10.1016/j.compag.2023.107746>
- Bai, Y., Fang, Y., Zhang, B., & Fan, S. (2022). Model robustness in estimation of blueberry SSC using NIRS. *Computers and Electronics in Agriculture*, 198, Article 107073. <https://doi.org/10.1016/j.compag.2022.107073>
- Balabin, R. M., & Safieva, R. Z. (2011). Biodiesel classification by base stock type (vegetable oil) using near infrared spectroscopy data. *Analytica Chimica Acta*, 689(2), 190–197. <https://doi.org/10.1016/j.aca.2011.01.041>
- Barra, I., Briak, H., & Kebede, F. (2022). The application of statistical preprocessing on spectral data does not always guarantee the improvement of the predictive quality of multivariate models: Case of soil spectroscopy applied to Moroccan soils. *Vibrational Spectroscopy*, 121, Article 103409. <https://doi.org/10.1016/j.vibspec.2022.103409>
- Becerra-Martínez, E., Florentino-Ramos, E., Pérez-Hernández, N., Gerardo Zepeda-Vallejo, L., Villa-Ruano, N., Velázquez-Ponce, M., & Bañuelos-Hernández, A. E. (2017). 1H NMR-based metabolomic fingerprinting to determine metabolite levels in serrano peppers (*Capsicum annum* L.) grown in two different regions. *Food Research International*, 102, 163–170. <https://doi.org/10.1016/j.foodres.2017.10.005>
- Bian, X., Xie, X., Cai, J., Zhao, Y., Miao, W., Chen, X., & Wu, J. L. (2022). Dynamic changes of phenolic acids and antioxidant activity of Citri Reticulatae Pericarpium during aging processes. *Food Chemistry*, 373(Pt A), Article 131399. <https://doi.org/10.1016/j.foodchem.2021.131399>
- Cruz Ulloa, C., Krus, A., Barrientos, A., Cerro, J. d., & Valero, C. (2022). Robotic fertilization in strip cropping using a CNN vegetables detection-characterization method. *Computers and Electronics in Agriculture*, 193, Article 106684. <https://doi.org/10.1016/j.compag.2022.106684>
- Dong, R., Wang, J., Weng, S., Yuan, H., & Yang, L. (2021). Field determination of hazardous chemicals in public security by using a hand-held Raman spectrometer and a deep architecture-search network. *Spectrochimica Acta Part A: Molecular and Biomolecular Spectroscopy*, 258, Article 119871. <https://doi.org/10.1016/j.saa.2021.119871>
- Du, H., Chen, W., Lei, Y., Li, F., Li, H., Deng, W., & Jiang, G. (2021). Discrimination of authenticity of *Fritillariae Cirrhosae Bulbus* based on terahertz spectroscopy and chemometric analysis. *Microchemical Journal*, 168, Article 106440. <https://doi.org/10.1016/j.microc.2021.106440>
- Fuentes, C. A., Öztop, M. H., Rojas-Rioseco, M., Bravo, M., Göksu, A., Manley, M., & Castillo, R. D. P. (2023). Application of segmented analysis via multivariate curve resolution with alternating least squares to 1H-nuclear magnetic resonance spectroscopy to identify different sugar sources. *Food Chemistry*, 428, Article 136817. <https://doi.org/10.1016/j.foodchem.2023.136817>
- Guo, Z., Zhang, Y., Wang, J., Liu, Y., Jayan, H., El-Seedi, H. R., & Zou, X. (2023). Detection model transfer of apple soluble solids content based on NIR spectroscopy and deep learning. *Computers and Electronics in Agriculture*, 212, Article 108127. <https://doi.org/10.1016/j.compag.2023.108127>
- Jiao, Y., Li, Z., Chen, X., & Fei, S. (2020). Preprocessing methods for near-infrared spectrum calibration. *Journal of Chemometrics*, 34(11), Article e3306. <https://doi.org/10.1002/cem.3306>
- Li, P., Zhang, X., Zheng, Y., Yang, F., Jiang, L., Liu, X., & Shan, Y. (2021). A novel method for the nondestructive classification of different-age Citri Reticulatae Pericarpium based on data combination technique. *Food Science & Nutrition*, 9(2), 943–951. <https://doi.org/10.1002/fsn3.2059>
- Li, Y., Fei, C., Mao, C., Ji, G. J., Qin, Y., & Lu, T. (2022). Physicochemical parameters combined flash GC e-nose and artificial neural network for quality and volatile characterization of vinegar with different brewing techniques. *Food Chemistry*, 374, Article 131658. <https://doi.org/10.1016/j.foodchem.2021.131658>
- Liu, M., Xiao, W., Zhang, H., & Sun, G. (2023). Quality control strategies of medicine food homology materials based on fingerprint profiling and chemometrics: Citri Reticulata Pericarpium as an example. *Spectrochimica Acta. Part A, Molecular and Biomolecular Spectroscopy*, 286, Article 121968. <https://doi.org/10.1016/j.saa.2022.121968>
- Liu, X., Zhang, S., Ni, H., Xiao, W., Wang, J., Li, Y., & Wu, Y. (2019). Near infrared system coupled chemometric algorithms for the variable selection and prediction of baicalin in three different processes. *Spectrochimica Acta Part A: Molecular and Biomolecular Spectroscopy*, 218, 33–39. <https://doi.org/10.1016/j.saa.2019.03.113>
- Luo, Y., Zeng, W., Huang, K. E., Li, D. X., Chen, W., Yu, X. Q., & Ke, X. H. (2019). Discrimination of Citrus reticulata Blanco and Citrus reticulata 'Chachi' as well as the Citrus reticulata 'Chachi' within different storage years using ultra high performance liquid chromatography quadrupole/time-of-flight mass spectrometry based metabolomics approach. *Journal of Pharmaceutical and Biomedical Analysis*, 171, 218–231. <https://doi.org/10.1016/j.jpba.2019.03.056>
- Ma, H., Shao, Y., Chen, J., Pan, D., Si, L., Liu, X., & Wu, Y. (2020). Maintaining the predictive abilities of near-infrared spectroscopy models for the determination of multi-parameters in White Paeony Root. *Infrared Physics & Technology*, 109, Article 103419. <https://doi.org/10.1016/j.infrared.2020.103419>
- Morais, C. L. M., Santos, M. C. D., Lima, K. M. G., & Martin, F. L. (2019). Improving data splitting for classification applications in spectrochemical analyses employing a random-mutation Kennard-Stone algorithm approach. *Bioinformatics*, 35(24), 5257–5263. <https://doi.org/10.1093/bioinformatics/btz421>
- Nasiri, A., Yoder, J., Zhao, Y., Hawkins, S., Prado, M., & Gan, H. (2022). Pose estimation-based lameness recognition in broiler using CNN-LSTM network. *Computers and Electronics in Agriculture*, 197, Article 106931. <https://doi.org/10.1016/j.compag.2022.106931>
- Pan, S., Zhang, X., Xu, W., Yin, J., Gu, H., & Yu, X. (2022). Rapid On-site identification of geographical origin and storage age of tangerine peel by Near-infrared spectroscopy. *Spectrochimica Acta. Part A, Molecular and Biomolecular Spectroscopy*, 271, Article 120936. <https://doi.org/10.1016/j.saa.2022.120936>

- Rong, D., Wang, H., Ying, Y., Zhang, Z., & Zhang, Y. (2020). Peach variety detection using VIS-NIR spectroscopy and deep learning. *Computers and Electronics in Agriculture*, 175, Article 105553. <https://doi.org/10.1016/j.compag.2020.105553>
- Wang, D., Jiang, J., Mo, J., Tang, J., & Lv, X. (2020). Rapid screening of thyroid dysfunction using Raman spectroscopy combined with an improved support vector machine. *Applied Spectroscopy*, 74(6), 674–683. <https://doi.org/10.1177/0003702820904444>
- Yi, L., Dong, N., Liu, S., Yi, Z., & Zhang, Y. (2015). Chemical features of Pericarpium Citri Reticulatae and Pericarpium Citri Reticulatae Viride revealed by GC-MS metabolomics analysis. *Food Chemistry*, 186, 192–199. <https://doi.org/10.1016/j.foodchem.2014.07.067>
- Yu, G., Ma, B., Chen, J., Li, X., & Li, C. (2020). Nondestructive identification of pesticide residues on the Hami melon surface using deep feature fusion by Vis/ NIR spectroscopy and 1D-NN. *Journal of Food Process*, (40).
- Yuan, Y.-Y., Wang, S.-T., Wang, J.-Z., Cheng, Q., Wu, X.-J., & Kong, D.-M. (2020). Rapid detection of the authenticity and adulteration of sesame oil using excitation-emission matrix fluorescence and chemometric methods. *Food Control*, 112, Article 107145. <https://doi.org/10.1016/j.foodcont.2020.107145>
- Zeng, J., Guo, Y., Han, Y., Li, Z., Yang, Z., Chai, Q., & Fu, C. (2021). A review of the discriminant analysis methods for food quality based on near-infrared spectroscopy and pattern recognition. *Molecules*, 26(3), 749. <https://www.mdpi.com/1420-3049/26/3/749>
- Zhan, H., Fang, J., Tang, L., Yang, H., Li, H., Wang, Z., & Fu, M. (2017). Application of near-infrared spectroscopy for the rapid quality assessment of Radix Paeoniae Rubra. *Spectrochimica Acta Part A: Molecular and Biomolecular Spectroscopy*, 183, 75–83. <https://doi.org/10.1016/j.saa.2017.04.034>
- Zhang, J.-B., Li, M.-X., Zhang, Y.-F., Qin, Y.-W., Li, Y., Su, L.-L., & Lu, T.-L. (2023). E-eye, flash GC E-nose and HS-GC-MS combined with chemometrics to identify the adulterants and geographical origins of Ziziphi Spinosae Semen. *Food Chemistry*, 424, Article 136270. <https://doi.org/10.1016/j.foodchem.2023.136270>
- Zhang, J., Li, Y., Wang, B., Song, J., Li, M., Chen, P., & Lu, T. (2023). Rapid evaluation of Radix Paeoniae Alba and its processed products by near-infrared spectroscopy combined with multivariate algorithms. *Analytical and Bioanalytical Chemistry*, 415(9), 1719–1732. <https://doi.org/10.1007/s00216-023-04570-5>
- Zhang, J., Wu, X., Qiu, J., Zhang, L., Zhang, Y., Qiu, X., & Xu, W. (2020). Comprehensive comparison on the chemical profile of Guang Chen Pi at different ripeness stages using untargeted and pseudotargeted metabolomics. *Journal of Agricultural and Food Chemistry*, 68(31), 8483–8495. <https://doi.org/10.1021/acs.jafc.0c02904>
- Zhang, X., Sun, J., Li, P., Zeng, F., & Wang, H. (2021). Hyperspectral detection of salted sea cucumber adulteration using different spectral preprocessing techniques and SVM method. *LWT*, 152, Article 112295. <https://doi.org/10.1016/j.lwt.2021.112295>